Synthesis of an Individualized Cranial Atlas with Dysmorphic Shape

Gary E. Christensen[12], Alex A. Kane[1], Jeffrey L. Marsh[12], and Michael W. Vannier[21]
Department of Surgery[1] and Mallinckrodt Institute of Radiology[2]
Washington University School of Medicine, St. Louis, Missouri 63110

Abstract

A new method for non-rigid registration of a normal infant CT head atlas with CT data of infants with abnormal skull shape is presented. An individualized atlas is synthesized by computing a volume transformation from the normal atlas to the target data set shape. This process begins rigidly by eliminating translation and rotation differences and proceeds non-rigidly to eliminate anatomical shape differences. Operator specified anatomical landmarks are used to find the initial rigid transformation. Non-rigid registration is achieved by constraining the transformation by the low frequency modes of vibration of a 3D linear-elastic solid while minimizing the squared intensity difference between atlas and target CT image volumes. Results are presented in which the CT atlas was transformed into the shape of several infants with various types of craniofacial deformities.

1. Introduction

Electronic atlases of normal individuals have been generated for several adults, especially in the head by Höhne [11], and for the entire human body as part of the National Library of Medicine Visible Human Project [18]. Electronic atlases of the head in infants and children, especially those with cranial deformities, have not been reported.

Tools that adapt a normal electronic atlas to match a specific individual wherein the atlas is transformed volumetrically to the target individual's shape have emerged and found application in neuromorphometry [2, 10], multimodality fusion [15], and locating regions of interest [3, 6, 7, 8, 17].

Atlas matching tools which produce an individualized labeled volume avoid the necessity for tedious and error prone segmentation and labeling. In general, these tools have been applied only in data sets from mature normal adults.

This paper reports on development of new methodology to synthesize individualized atlases corresponding to well known types of major craniofacial deformities, including sagittal synostosis, bilateral coronal synostosis, and unilateral coronal synostosis. Since these deformities are usually treated with surgery in infancy or early childhood, a new electronic CT atlas of the head was created using scans from a three month old female whose skull shape was normal.

The goal of this study was to test extensions of previously developed tools [3, 15] based on Grenander's global shape models [9] in craniofacial dysmorphology. Specifically, we sought to test the feasibility of generating electronic atlases in cases with major skull deformities and evaluate the quality of the results.

If successful, individualized atlases of dysmorphic individuals could simultaneously provide automatic segmentation and labeling of craniofacial anatomy as well as a quantitative description of the dysmorphic features thereby facilitating treatment and evaluation.

2. Problem Statement

An anatomical atlas is an annotated collection of images, charts, or tables that systematically illustrates biological structure for all or part of an organism. In our case, the atlas is a spatial array of CT scan data (voxel-based attenuation measurements with associated tissue type (bone or not bone) and labels derived from a volumetric CT scan of a normal 3 month old female head. The atlas annotations (knowledge base) provide a basis for understanding the relevant anatomy. However, due to the labor intensive nature of creating an atlas knowledge base, only one atlas from a population is usually produced. This paper addresses the problem of synthesizing individualized atlases given a target CT data set and a topologically equivalent electronic atlas. The atlas is individualized by finding the transformation that changes its shape to match the target CT volume and then using that transformation to map the atlas knowledge base onto the target CT volume as shown

in Fig. 1. In addition, the atlas transformation can be used to quantitatively assess the absolute shape characteristics of the target CT as well as its shape differences compared to the atlas. It is therefore possible to use the atlas transformation to locate and measure areas of abnormality in the target CT data set. Ideally, synthesizing an individualized atlases in this manner can provide the following information regarding a patient's anatomy based their on CT data set.

Individualized Atlas

- Bone and soft-tissue segmentation
- Anatomical landmarks and suture locations
- Geometric information such as distances, angles, volumes, and curvatures
- Connectivity
- Text description of dysmorphology
- Treatment options and procedures
- Links to relevant medical literature

Atlas Transformation

- Location of abnormality
- Magnitude of abnormality
- Shape of abnormality
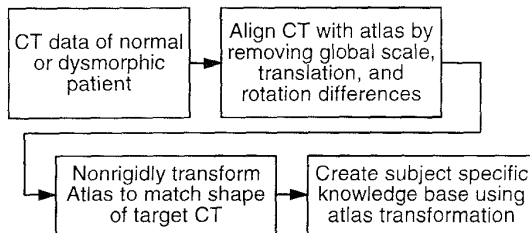- Measure of asymmetry
- Change in shape

Figure 1. Synthesis of an Individualized Atlas.

The atlas is described mathematically on the domain Ω as a vector valued function $A(x) = (A_1(x), \ldots, A_N(x))$ for $x \in \Omega \subset R^3$. The modality A_1 corresponds to a 3D CT data set of the atlas anatomy where the other $N - 1$ modalities correspond to the knowledge base of the atlas, i.e., A_2 could correspond

to a bone segmentation, A_3 could correspond to a collection of anatomical landmarks, etc. The notation T will be used to represent the CT modality of the atlas and is referred to as the template.

Problem Statement: Given a target CT data set $S(x)$, find the optimal transformation $h(x)$ in some sense that transforms the shape of the atlas template $T(x)$ into that of $S(x)$ while maintaining the topology of $T(x)$ for $x \in \Omega$. The individualized atlas is generated by applying the transformation h to the atlas A, i.e., the individualized atlas is given by $A(h(x))$.

3. Construction of the Atlas

The construction of the atlas consisted of defining the atlas coordinate system, selecting a data set for the atlas, and defining the information in the atlas knowledge base.

3.1. The Atlas Coordinate System

The first step in constructing an atlas requires definition of the coordinate system, a reference frame that assigns each anatomic structure a specific location. The reference system facilitates measurement of distances and angles between standardized anatomic (cephalometric) landmarks, curvatures, volumes, and other shape measures.

The atlas coordinate system is defined by an origin and three orthonormal basis vectors. The coordinate system was defined to correspond to the normals of the Frankfort Horizontal plane (FH), the Median Sagittal or MidSagittal Plane (MSP), and the Coronal Plane, see Figs. 2 and 3. The FH is a horizontal plane represented in profile by a line between the *orbitale*, the lowest point on the margin of the orbit, and the *porion*, the highest point on the margin of the auditory meatus. Its definition as the standard orientation for depicting human skulls was initially adopted at the 13th General Congress of German Anthropologists (the "Frankfort Agreement"), Frankfurt-am-Main, 1882, and subsequently by the International Agreement for the Unification of Craniometric and Cephalometric Measurements, Monaco, 1906 [12]. The MSP is perpendicular to the FH and is defined as the plane of symmetry that passes through the head from front to back dividing it into right and left halves. The Coronal Plane is defined perpendicular to the FH and MSP dividing the head into anterior and posterior parts.

The origin of the coordinate system was selected as the *basion*, the midpoint of the anterior border of the foramen magnum in the midsagittal plane (see Fig. 2). This point was chosen because it is almost always

Figure 2. Front, side, and bottom views of the 3 month old infant, CT atlas skull. Landmarks: 1. prosthion, 2. subnasale, 3. rhinion, 4. nasale, 5. top of metopic suture, 6. bregma, 7. lambda, 8. opisthocranion, 9. basion, 10. right orbitale, 11. left orbitale, 12. right porion. Bones: 13. & 14. R./L. frontal bone, 15. & 16. R./L. maxilla, 17. & 18. R./L. mandible, 19. & 20. R./L. temporal bone, 21. & 22. R./L. parietal bone, 23. occipital bone, 24. sphenoid bone, 25. vertebral column. 26. R. zygomatic bone.

3.2. The Atlas CT Data

A CT data set of a normal 3 month old female was chosen as the atlas template and was selected from the craniofacial image archive at the Cleft Palate and Craniofacial Deformities Institute (CPCDI) of St. Louis Children's Hospital at Washington University Medical Center. This data was collected using a Siemens Splus S Spiral CT scanner at $0.49 \times 0.49 \times 2.0$ mm^3 resolution forming a $512 \times 512 \times 82$ voxel volume.

The CT data volume was aligned with the atlas coordinate system using the rigid registration procedure described in Section 4.1. In this procedure, the CT data was resampled such that the voxel lattice of the new CT volume corresponded to the Frankfort horizontal, midsagittal, and coronal planes of the data.

The CT data is stored in the atlas at three different resolutions—low, medium, and high—corresponding to voxel dimensions of $1.96 \times 1.96 \times 2.0$, $0.98 \times 0.98 \times 1.0$, and $0.49 \times 0.49 \times 0.49$ mm^3, respectively, in a $251 \times 251 \times 200$ mm^3 domain Ω. The low resolution $128 \times 128 \times 100$ voxel volume was used as the template for individualizing the atlas; the medium resolution $256 \times 256 \times 200$ voxel volume was used to visualize the atlas CT before and after transformation; and the high resolution volume (stored as a $285 \times 345 \times 335$ voxel subvolume) was used to create precise manual segmentations of the atlas anatomy and for generating high resolution segmentations of the target CT data sets.
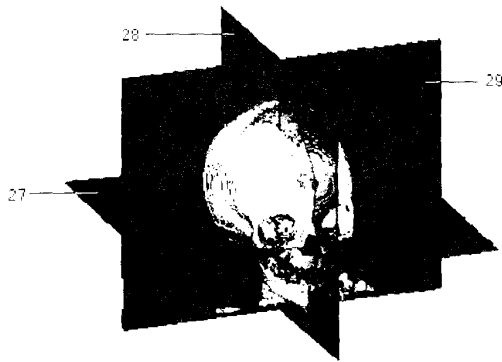

Figure 3. Coordinate system of 3 month old infant, CT atlas skull. Planes: 27. Frankfort horizontal plane, 28. medial sagittal plane, 29. coronal plane.

present in normal and abnormal anatomies. Another possible choice for the origin is the center of the sella turcica which is used in a majority of the cephalometric literature. This point was not used due to the difficulty in trying to locate the center of this cup-like structure in 3D [16].

3.3. The Atlas Knowledge Base

The atlas knowledge base for this project consisted of 13 landmark coordinates and the segmentations of 17 major bones of the skull (see Figure 2). The bone segmentations were generated by careful manual segmentation performed by an anatomic expert (A.A.K.) using Analyze^{TM} software. The CT data was converted from 16-bit to 8-bit data by linearly mapping the intensity range of 600-2200 to 0-255; intensities below 600 where mapped to zero, and intensities above 2200 were mapped to 255. Bone was segmented from soft-tissue using a threshold of 85-255 and manually partitioned into individual skull bones. In the future, additional structures will be added to the knowledge base as needed.

4. Individualizing the Atlas

The atlas is individualized for a particular target CT data set using a two-step process as shown in Fig 1. First, a rigid transformation s applied that removes rotation and translation differences between the target and the atlas. Next, a non-rigid transformation based on a linear-elastic solid model is used to accommodate anatomical shape differences between the target data set and the atlas.

4.1. Rigid Registration

Rigid registration of a CT data set to the atlas coordinate system consists of finding a translation vector and a rotation matrix. The translation vector is determined by computing the difference between the coordinates of the origin in the atlas and the corresponding landmark in the target data set.

The rotation matrix is determined by estimating the equations of the Frankfort horizontal, midsagittal, and coronal planes in the CT data set and calculating the three angles required to rotate these orthogonal planes onto the voxel lattice. Landmarks are used to define points on one of the three planes and least-squares estimation is used to estimate the equation of a plane that best fits the landmarks. The second plane is found in a similar manner but is constrained to be perpendicular to the first. The orientation of the third plane is constrained to be perpendicular to the first two planes and is therefore completely determined by the first two planes There are six different possible orderings for determining the equations of the planes, each of which gives a slightly different procedure for finding the rotation matrix. Rather than enumerating all six procedures, only the case corresponding to finding the MSP

first and the FH second is presented. The procedures for the other five cases can be derived in a similar manner.

The transformation that rigidly registers a CT data set to the atlas coordinate system finding the MSP followed by the FH can be written as

$$q = R_x R_y R_z (p - p_0) + p_1 \qquad (1)$$

where

$$R_x = \begin{bmatrix} 1 & 0 & 0 \\ 0 & \cos\phi & \sin\phi \\ 0 & -\sin\phi & \cos\phi \end{bmatrix}, \quad R_y = \begin{bmatrix} \cos\theta & 0 & \sin\theta \\ 0 & 1 & 0 \\ -\sin\theta & 0 & \cos\theta \end{bmatrix},$$

$$R_z = \begin{bmatrix} \cos\gamma & \sin\gamma & 0 \\ -\sin\gamma & \cos\gamma & 0 \\ 0 & 0 & 1 \end{bmatrix},$$

are rotation matrices about the x, y, and z-axis, respectively. Points $p = [x, y, z]$ are mapped to points $q = [x', y', z']$ and $p_1 = [x_1, y_1, z_1]$ is the origin of the atlas and $p_0 = [x_0, y_0, z_0]$ is the origin in the target data set. The angles ϕ, θ, and γ rotate the data set so its data voxel lattice corresponds to its Frankfort horizontal plane (FH), midsagittal plane (MSP), and coronal plane. Notice that the translation vector aligns the origin of the data set with that of the atlas anatomy.

In a normal anatomy the landmarks that define the FH are the porions and the orbitales; the landmarks used to define the MSP were the prosthion, subnasale, rhinion, nasale, the top of the metopic suture, bregma, lambda, opisthocranion, and basion (see Fig. 2). Finding landmarks to define the FH and MSP is more complicated for dysmorphic (abnormal) skulls, due to asymmetries and missing landmarks. For the SS and BCS results presented in Section 5, all of the landmarks above were used to define the FH and MSP due to the symmetry of these deformities. However due to the asymmetry of the UCS data set, only the prosthion, subnasale, and basion were used to define the MSP and the left porion and left orbitale were used to define the FH.

The equation of the MSP is determined as follows. Let the set $\{(x_1, y_1, z_1), \dots (x_n, y_n, z_n)\}$ denote the coordinates of the n landmarks used to define the MSP. The equation of the MSP can be written as $ax + by + cz = d$ where $a + b + c = 1$. Combining these equations, we get n equations (one for each landmark) of the form $z_i - a(z_i - x_i) - b(z_i - y_i) - d = 0$ for determining the unknown constants a, b, and d. Provided that $n \geq 3$, we can formulate the following

least-squares problem

$$\min_v (u - Wv)^2 =$$

$$\min_{a,b,d} \left(\begin{bmatrix} z_1 \\ \vdots \\ z_n \end{bmatrix} - \begin{bmatrix} (z_1 - x_1) & (z_1 - y_1) & 1 \\ \vdots & \vdots & \vdots \\ (z_n - x_n) & (z_n - y_n) & 1 \end{bmatrix} \begin{bmatrix} a \\ b \\ d \end{bmatrix} \right)^2. \quad (2)$$

The solution of this minimization problem is

$$\hat{v} = (W^T W)^{-1} W^T u \quad (3)$$

(see pg. 83 of Luenberger [14]). Using this estimate of a, b, and c, we can find the angles θ and γ that rotate the MSP plane such that its normal vector (a, b, c) is aligned parallel to the x-axis, i.e.,

$$\begin{bmatrix} \cos\theta & 0 & \sin\theta \\ 0 & 1 & 0 \\ -\sin\theta & 0 & \cos\theta \end{bmatrix} \begin{bmatrix} \cos\gamma & \sin\gamma & 0 \\ -\sin\gamma & \cos\gamma & 0 \\ 0 & 0 & 1 \end{bmatrix} \begin{bmatrix} a \\ b \\ c \end{bmatrix}$$

$$= \begin{bmatrix} \cos\theta & 0 & \sin\theta \\ 0 & 1 & 0 \\ -\sin\theta & 0 & \cos\theta \end{bmatrix} \begin{bmatrix} a' \\ 0 \\ c \end{bmatrix} = \begin{bmatrix} a'' \\ 0 \\ 0 \end{bmatrix}. \quad (4)$$

The solution of this equation is

$$\gamma = \tan^{-1}\left(\frac{b}{a}\right) \quad \text{and} \quad \theta = \tan^{-1}\left(\frac{c}{a'}\right) \quad (5)$$

where $a' = a\cos\gamma + b\sin\gamma$.

The equation of the FH plane can now be determined as follows. Let $\{(x_1, y_1, z_1), \ldots (x_m, y_m, z_m)\}$ denote the coordinates of the m landmarks used to define the FH. These landmarks are rotated by θ and γ to get the new coordinates in which the MSP is perpendicular to the x-axis, i.e.,

$$\begin{bmatrix} \tilde{x}_i \\ \tilde{y}_i \\ \tilde{z}_i \end{bmatrix} = \begin{bmatrix} \cos\theta & 0 & \sin\theta \\ 0 & 1 & 0 \\ -\sin\theta & 0 & \cos\theta \end{bmatrix} \begin{bmatrix} \cos\gamma & \sin\gamma & 0 \\ -\sin\gamma & \cos\gamma & 0 \\ 0 & 0 & 1 \end{bmatrix} \begin{bmatrix} x_i \\ y_i \\ z_i \end{bmatrix}$$

The equation of the FH plane can be written as $ax + by + cz = d$ where $a + b + c = 1$ and $a = 0$. The condition $a = 0$ ensures that the FH plane will be perpendicular to the MSP. Combining these equations, we get m equations of the form $\tilde{z}_i - b(\tilde{z}_i - \tilde{y}_i) - d = 0$. Provided that $m \geq 2$, the least-squares estimate of FH is given by

$$\min_v (u - Wv)^2 = \min_{b,d} \left(\begin{bmatrix} z_1 \\ \vdots \\ z_m \end{bmatrix} - \begin{bmatrix} (z_1 - y_1) & 1 \\ \vdots & \vdots \\ (z_m - y_m) & 1 \end{bmatrix} \begin{bmatrix} b \\ d \end{bmatrix} \right)^2$$

which has solution given by Eq. 3. The angle ϕ that rotates the FH such that its normal $(0, b, c)$ is parallel

to the z-axis satisfies

$$\begin{bmatrix} 1 & 0 & 0 \\ 0 & \cos\phi & \sin\phi \\ 0 & -\sin\phi & \cos\phi \end{bmatrix} \begin{bmatrix} 0 \\ b \\ c \end{bmatrix} = \begin{bmatrix} 0 \\ 0 \\ c' \end{bmatrix}$$

implying

$$\phi = \tan^{-1}\left(-\frac{b}{c}\right). \quad (6)$$

4.2. Non-Rigid Registration Using a Linear-Elastic Model

Non-rigid registration of the atlas is accomplished by finding the displacement field $u(x) = x - h(x)$ that minimizes the energy functional

$$E_1(u) = \frac{1}{2\sigma^2} \int_\Omega (T(x - u(x)) - S(x))^2 dx$$

$$+ \frac{1}{2} \int_\Omega |Lu(x)|^2 dx \quad (7)$$

where σ is a constant and L is a linear operator. The first term on the right-hand-side corresponds to a cost of the intensity mismatch between the template and target CT volume. The second term is a regularization term that maintains the topology of the template by penalizing rough displacement fields. We simplify Eq. 7 by representing u by its eigenfunction decomposition $u(x) = \sum_{i=1}^d \mu_i \phi_i(x)$ where $L\phi_i(x) = \lambda_i \phi_i(x)$. The functions ϕ_i are the eigenfunctions of L and have eigenvalue λ_i. Substituting the eigenfunction expansion of u into Eq. 7 gives a new energy function

$$E_2(\mu) = \frac{1}{2\sigma^2} \int_\Omega (T(x - u(x)) - S(x))^2 dx + \frac{1}{2} \sum_{i=1}^d \lambda_i^2 \mu_i^2$$

in terms of the coefficients $\mu = [\mu_1, \ldots, \mu_d]^T$. The problem now becomes that of finding μ that minimizes $E_2(\mu)$. The solution of this problem is found by gradient decent

$$\mu_i^{k+1} = \mu_i^k - \Delta[S(x) - T(x - u(x))] \left.\frac{\partial T}{\partial \mu_i}\right|_{x - u(x)}$$

$$- \Delta \lambda_i^2 \mu_i \quad (8)$$

The linear operator L used in this work was the linear elastic operator $Lu(x) = \alpha\nabla^2 u(x) + \beta\nabla(\nabla \cdot u(x))$ with boundary conditions $\left.\frac{\partial u_i}{\partial x_i}\right|_{(x|x_i=k)} = u_i(x|x_j = k) = 0$ for $i, j = 1, 2, 3$; $i \neq j$; $k = 0, 1$; and $x \in \Omega = [0, 1]^3$. The notation $(x|x_i = k)$ is defined as $x \in \Omega$ such that $x_i = k$, $\nabla = [\frac{\partial}{\partial x_1}, \frac{\partial}{\partial x_1}, \frac{\partial}{\partial x_1}]$, and

$\nabla^2 = \nabla \cdot \nabla$. Thus as first reported in [3], the displacement field has the form

$$u(x) = \sum_{n=1}^{3} \sum_{\nu \in S(d)} \mu_{n,\nu} \phi_{n,\nu}(x). \qquad (9)$$

where

$$S(d) = \{(i,j,k) \mid i+j+k > 0 \quad \text{and} \quad 0 \le i,j,k, \le d\}$$

$$\phi_{1,\nu}(x) = \eta_1 [ig_{1,\nu}(x), jg_{2,\nu}(x), kg_{3,\nu}(x)]^T$$
$$\phi_{2,\nu}(x) = \eta_2 [-jg_{1,\nu}(x), ig_{2,\nu}(x), 0]^T$$
$$\phi_{3,\nu}(x) = \eta_3 [ikg_{1,\nu}(x), jkg_{2,\nu}(x), -(i^2+j^2)g_{3,\nu}(x)]^T$$

$$g_{1,\nu}(x) = \cos i\pi x_1 \sin j\pi x_2 \sin k\pi x_3$$
$$g_{2,\nu}(x) = \sin i\pi x_1 \cos j\pi x_2 \sin k\pi x_3$$
$$g_{3,\nu}(x) = \sin i\pi x_1 \sin j\pi x_2 \cos k\pi x_3 \qquad (10)$$

$\eta_1 = \sqrt{8/(i^2+j^2+k^2)}$, $\eta_2 = \sqrt{8/(i^2+j^2)}$, and $\eta_3 = \eta_1\eta_2\sqrt{1/8}$. The eigenvalues for $\phi_{n,\nu}$ are $\lambda_{1,\nu} = -\pi^2(2\alpha+\beta)(i^2+j^2+k^2)$ and $\lambda_{2,\nu} = \lambda_{3,\nu} = -\pi^2\alpha(i^2+j^2+k^2)$. A limitation of this model and others such as the membrane model $Lu(x) = \nabla^2 u(x)$ or the bi-harmonic model $Lu(x) = \nabla^4 u(x)$ is that they are only valid for small deformations [1]. These limitations can be overcome using a fluid model [4] for atlas transformations requiring large nonlinear deformations.

This minimization problem can be interpreted probabilistically as the maximum a posteriori estimate of μ for the density $p(\mu) = \frac{1}{Z}e^{-E_2(\mu)}$. It is also possible to find the conditional mean estimate of μ as in [3, 15].

The parameters used to generate the experimental results were $\sigma = 0.01$, $\alpha = 0.1$, and $\beta = 0$. The template and study intensities were normalized from 0-255 to 0-1. The gradient decent Eq. 8 was run for 300 iterations; $d = 1$ initially and $d = d + 1$ every 40 iterations which gave a final transformation with 2187 degrees of freedom. Increasing the number of basis functions allows a multiresolution solution that matches larger structures before smaller structures and requires less computation time then if all 300 iterations were performed for $d = 8$. The step size of the gradient decent was normalized as the number of basis functions was increased by setting $\Delta = 2.0 \times 10^{-11} \times (\sum_{n=1}^{3}\sum_{\nu \in S(d)} \lambda_{n,\nu}^2)^{-1}$. The computation of the linear-elastic transformation for the $128 \times 128 \times 100$ voxel template and study required approximately 2.75 hours using a 128×128 MasPar MP-2 massively parallel computer. All final transformations had a globally positive Jacobian over Ω and therefore preserved the topology of the template [5].

5. Results

Three individualized atlases of infants with abnormal skull shapes were generated to test the atlas registration algorithm. Figures 4, 5, and 6 show the skull of the target CT data volumes (top row) and the skull of the transformed atlas (bottom row) for the craniofacial deformities of sagittal, bilateral coronal, and unilateral coronal synostosis. Abnormal skull shape due to sagittal synostosis (SS) is characterized by an anterior-posterior elongation and left-right narrowing of the skull. Abnormal skull shape due to bilateral coronal synostosis (BCS) is characterized by an anterior-posterior shortening and left-right widening of the skull. In contrast to SS and BCS skull shapes which are relatively symmetric about the midsagittal plane, unilateral coronal synostosis (UCS) skull shape is asymmetric about the midsagittal plane.
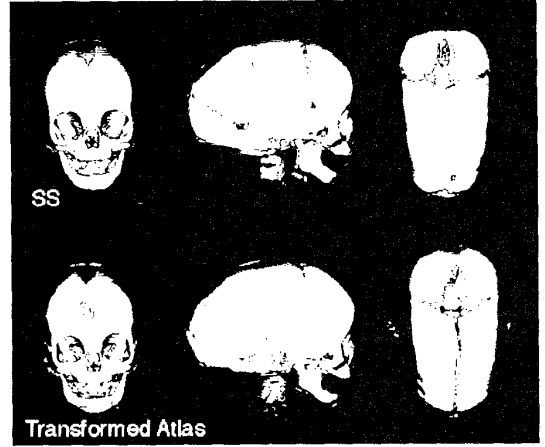

Figure 4. Front, right, and top views of the skull of an infant with sagittal synostosis (top row) and the skull of the transformed atlas (bottom row). Note: This transformation was constrained only to match bone and soft tissue in the CT volumes and not the sutures (the gaps between bones). Therefore, the shape of the transformed atlas skull matches very well with the shape of the patient skull, but the sutures do not necessarily match.

Visual inspection of the individualized atlases in these figures shows a good correspondence between the ensemble skull shape of the target data set and the individualized atlas. This demonstrates that the linear-elastic model had enough degrees of freedom to match
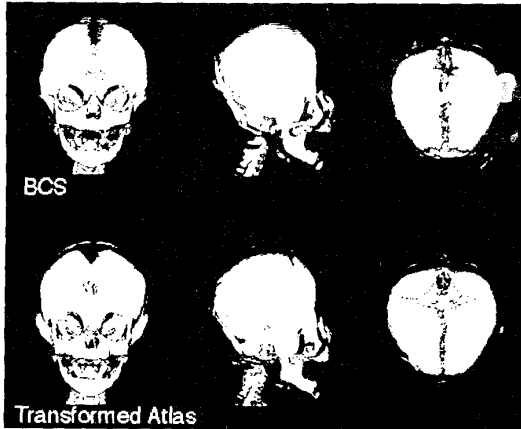
314

Figure 5. Front, right, and top views of the skull of an infant with bilateral coronal synostosis (top row) and the skull of the transformed atlas (bottom row). See note in Fig. 4.
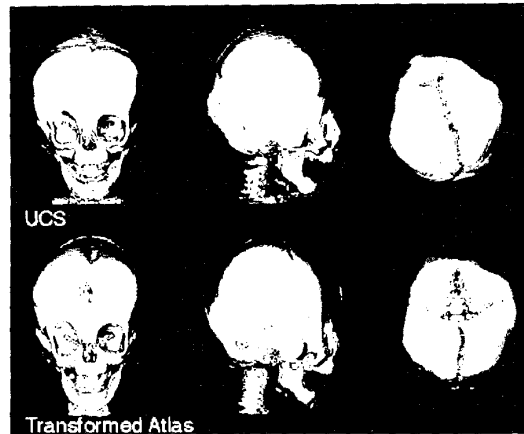

Figure 6. Front, right, and top views of the skull of an infant with unilateral coronal synostosis (top row) and the skull of the transformed atlas (bottom row). See note in Fig. 4.

the ensemble shape of the three abnormally shaped skulls. Notice that even the shape of the orbits of the individualized UCS atlas matches the shape of the orbits in the UCS target data set. These results also demonstrate that it is possible to transform an atlas of a normal infant head into the shape of an abnormal infant head in these three cases.

The intensity absolute error performance of the matching algorithm was determined quantitatively and visually. Table 1 tabulates the intensity absolute difference between the target CT volume and the atlas template CT volume before and after transformation. Notice that the intensity absolute difference was reduced to approximately 25 % of its original value after transformation. Figure 7 shows the absolute difference images between the target CT data set and the atlas before (top row) and after transformation (bottom row) for the BCS individualized atlas. This figure demonstrates that the reduction of the absolute difference to 25 % of its original value is enough to give good alignment of the the target and individualized template data sets. If a better alignment of the atlas and target is required, a higher dimensional transformation such as described in [4] could be used to refine these linear-elastic transformations.

Figures 4, 5, and 6 also demonstrate that the atlas registration method described in this paper does not accommodate the shape of each individual skull bone. This can be seen by comparing the skull sutures (the

Table 1. Performance of Registration

Experiment	Normalized Intensity Absolute Error		
	Before	After	% difference
Atlas to SS	1.54×10^5	4.38×10^4	28.4
Atlas to BCS	2.28×10^5	3.55×10^4	15.6
Atlas to UCS	2.07×10^5	5.40×10^4	26.1

gaps between the bones of the skull) of the individualized atlas and the target CT data set. Notice that none of the sutures necessarily agree between the target and the atlas. This limitation is expected because the similarity energy or cost (see Eq. 7) used to match the atlas and target is only a function of CT volume intensity. Therefore only subvolume differences between the atlas template and target contribute to the matching energy. Substructures such as points, lines, and surfaces have zero measure (zero energy) in this volume integral and thus have no effect on the the matching procedure. In the future, we intend to overcome this limitation by adding constraints to the transformation that match landmarks and sutures [13].

Another observation that can be made from these figures is that the individualized atlas contains all of the skull sutures while the target data sets do not.
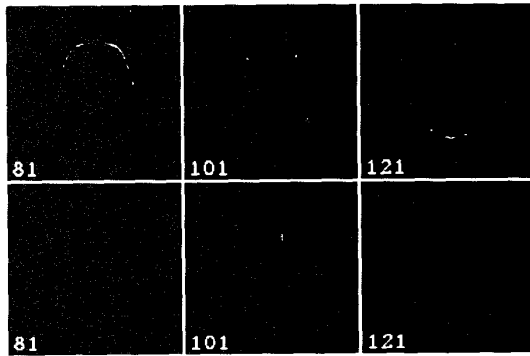
Figure 7. Top row shows absolute difference subtraction images between the untransformed atlas and BCS patient (see Fig. 5) for 3 axial slices. Bottom row shows the absolute difference subtraction images between the transformed atlas and BCS patient for the same 3 slices as the top row.

Each of the three abnormalities shown are caused by fusion (obliteration) of one or more sutures which therefore is (are) missing in the target. The sagittal suture is missing in SS, both coronal sutures are missing in BCS, and one of the coronal sutures is missing in UCS. The reason that the all of the sutures are present in the individualized atlases is that all of the sutures are present in the atlas and therefore must be present in the transformed atlas because of the topology preserving nature of the transformation.

Selected slices of the 3D displacement fields that generated the SS, BCS, and UCS individualized atlases are shown in Figures 8, 9, and 10, respectively. The top, middle, and bottom rows of these figures show the x, y, and z-components of the atlas transformation, respectively, superimposed on the corresponding axial CT slices of the target data set. White corresponds to a large positive displacement, medium-gray to zero displacement, and black to a large negative displacement. These transformation images can be interpreted in the following manner. In Figure 8, the x-component of slice 81 (top row) shows that the atlas was compressed left-to-right, the y-displacement of slice 81 (middle row) shows the atlas was stretched front-to-back, and the z-component (bottom row) shows no displacement top-to-bottom for the atlas to match the patient data.

Comparison of the y-displacement fields of Figures 8 and 9 shows that these displacements are inverted accounting for the elongation front-to-back in the SS individualized atlas and the compression front-to-back

in the BCS individualized atlas. The asymmetry of the displacement fields in Figure 10 were necessary to generate the asymmetry of the UCS individualized atlas.

These volume transformation give a quantitative measure of the distance from each point in the target to a corresponding point in the atlas; they therefore measure the shape change between the target and the atlas. Future work is planned that will use these volume transformations to measure and quantify abnormal anatomical shapes.
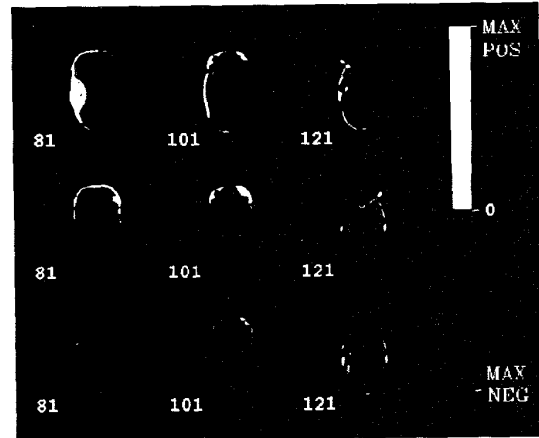

Figure 8. The atlas was compressed left-to-right, stretched front-to-back, and had very little displacement top-to-bottom for the atlas to match the patient data shown in Fig. 4. Key: Top, middle, and bottom rows show the x, y, and z-components of the atlas transformation, respectively, superimposed on three axial CT slices of the patient. The CT slices go from top to bottom of the head as the slice number increases. White corresponds to a large positive displacement and black to a large negative displacement.

Finally, Figure 11 shows the automatic segmentation generated for the SS individualized atlas. This segmentation was generated by applying the atlas transformation to the knowledge base of the atlas. This figure is intended to demonstrate the feasibility of mapping the atlas knowledge base and not as an accurate segmentation of the bones in the target data set. In the future when the individual bones of the atlas are constrained to match the corresponding bone in the target (see above), the automatic segmentation should give a precise segmentation of the bones in the target data set.
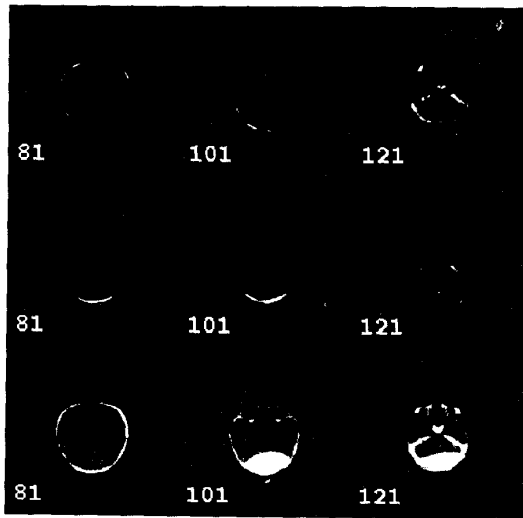
316

Figure 9. The atlas was compressed front-to-back, slightly compressed left-to-right, and the bottom-rear of the skull was displaced up for the atlas to match the patient data shown in Fig. 5. See key in Fig. 8.
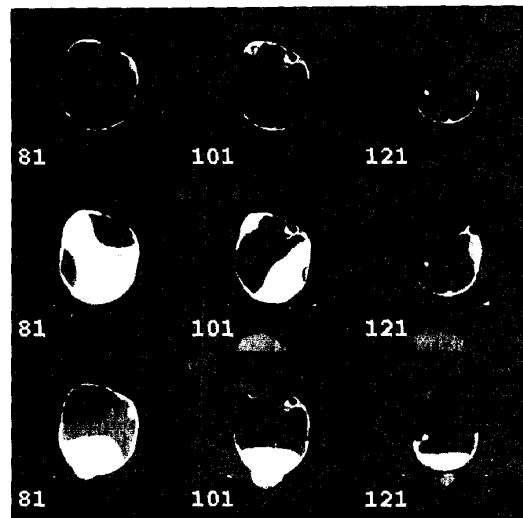
6. Summary and Conclusions

After applying the new method for nonrigid registration of the normal female infant's CT head atlas to the CT data sets of infants with abnormal skull shape, the results were displayed visually and the moduli for displacement fields computed and viewed in multiplanar displays. Operator specification of anatomic landmarks demonstrated a high degree of consistency along the target and transformed atlases showing that the procedure is robust to even high degrees of skull asymmetry.

7. Acknowledgments

References

[1] R. Bisplinghoff, J. Marr, and T. Pian. *Statics of Deformable Solids*. Dover Publications, Inc., 1965.

[2] F. Bookstein. *Morphometric Tools for Landmark Data*. Cambridge University Press, New York, 1991.

Figure 10. The transformation of the atlas to match the patient data shown in Fig. 6. Notice that the only x-displacement (top row) occured at the top-right portion of the skull, the asymmetry of the y-displacement (middle row) results from the asymmetry of the patient's skull, and the z-displacement (bottom row) shows that the back of the skull was lifted up while the front of the skull was pushed down. See key in Fig. 8.

[3] G. Christensen, R. Rabbitt, and M. Miller. 3D brain mapping using a deformable neuroanatomy. *Physics in Medicine and Biology*, 39:609–618, 1994.

[4] G. Christensen, R. Rabbitt, and M. Miller. Deformable templates using large deformation kinematics. *IEEE Transactions on Image Processing*, To appear in September, 1996.

[5] G. Christensen, R. Rabbitt, M. Miller, S. Joshi, U. Grenander, T. Coogan, and D. V. Essen. Topological properties of smooth anatomic maps. In Y. Bizais, C. Braillot, and R. D. Paola, editors, *Information Processing in Medical Imaging*, volume 3, pages 101–112. Kluwer Academic Publishers, Boston, June 1995.

[6] R. Dann, J. Hoford, S. Kovacic, M. Reivich, and R. Bajcsy. Evaluation of Elastic Matching Systems for Anatomic (CT, MR) and Functional (PET) Cerebral Images. *Journal of Computer Assisted Tomography*, 13(4):603–611, July/August 1989.

[7] A. Evans, W. Dai, D. Collins, P. Neelin, and S. Marret. Warping of a computerized 3-d atlas to match brain image volumes for quantitative neuroanatomical and functional analysis. *Image Processing*, SPIE 1445:236–246, 1991.

Figure 11. Individualized atlas for sagittal synostosis provides automatic segmentation and labeling (original in color to denote labels of each cranial bone).

[8] T. Greitz, C. Bohm, S. Holte, and L. Eriksson. A computerized brain atlas: Construction, anatomical content, and some applications. *Journal of Computer Assisted Tomography*, 15(1):26–38, Janurary/February 1991.

[9] U. Grenander. *General Pattern Theory*. Oxford University Press, 1993.

[10] J. Haller, G. Christensen, S. Joshi, J. Newcomer, M. Miller, J. Csernansky, and M. Vannier. Hippocampal MR morphometry by pattern matching. *Radiology*, in press.

[11] K. Höhne, M. Bomans, M. Reimer, and R. Schubert. A 3D anatomical atlas based on a volume model. *IEEE Comput. Graphics Appl.*, 12(4):72–78, 1992.

[12] S. Jablonski. *Illustrated Dictionary of Dentistry*. W.B. Saunders Company, Philadelphia, 1982.

[13] S. C. Joshi, M. I. Miller, G. E. Christensen, A. Banerjee, T. A. Coogan, and U. Grenander. Hierarchical brain mapping via a generalized dirichlet solution for mapping brain manifolds. *Vision Geometry IV*, SPIE 2573:278–289, 1995.

[14] D. Luenberger. *Optimization by Vector Space Methods*. John Wiley and Sons, New York, 1969.

[15] M. Miller, G. Christensen, Y. Amit, and U. Grenander. Mathematical textbook of deformable neuroanatomies. *Proceedings of the National Academy of Sciences*, 90(24):11944–48, Dec. 1993.

[16] Y. Sagawara, K. Harii, and S. Hirabayashi. Analysis of craniofacial asymmetry using accurate three-dimenional coordinates on the skull. In K. H. et al., editor, *Transactions of the 11th Congress of the International Confederation of Plastic, Reconstructive and Aesthetic Surgery*, page 33. Kugler Publications, New York, 1995.

[17] S. Sandor and R. Leahy. Towards automated labelling of the cerebral cortex using a deformable atlas. In Y. Bizais, C. Braillot, and R. D. Paola, editors, *Information Processing in Medical Imaging*, volume 3, pages 127–138. Kluwer Academic Publishers, Boston, June 1995.

[18] V. Spitzer, M. Ackerman, A. Scherzinger, and D. Whitlock. The visible human male: A technical report. *Journal of the American Medical Informatics Association*, 3(2), Mar/Apr 1996.